Structure and Stabilizing Interactions of Casein Micelles Probed by High-Pressure Light Scattering and FTIR

ARTICLE *in* THE JOURNAL OF PHYSICAL CHEMISTRY B · FEBRUARY 2011

Impact Factor: 3.3 · DOI: 10.1021/jp107622d · Source: PubMed

4 AUTHORS, INCLUDING:

Ronald Gebhardt
Technische Universität München
49 PUBLICATIONS **470** CITATIONS
SEE PROFILE

Ulrich Kulozik
Technische Universität München
114 PUBLICATIONS **1,647** CITATIONS
SEE PROFILE

Wolfgang Doster
Technische Universität München
26 PUBLICATIONS **569** CITATIONS
SEE PROFILE

THE JOURNAL OF PHYSICAL CHEMISTRY B

ARTICLE

pubs.acs.org/JPCB

Structure and Stabilizing Interactions of Casein Micelles Probed by High-Pressure Light Scattering and FTIR

Ronald Gebhardt,[*,†,§] Naohiro Takeda,[§,∥] Ulrich Kulozik,[†,‡] and Wolfgang Doster[*,§]

[†]Chair for Food Process Engineering and Dairy Technology, and [‡]ZIEL Center of Nutrition and Food Research, Technology Section, Technische Universität München, Weihenstephaner Berg 1, D-85354 Freising-Weihenstephan, Germany

[§]Physik-Department, Technische Universität München, D-85748 Garching, Germany

[∥]Department of Applied Chemistry, Ritsumeikan University, Noji-Higashi, Kusatsu, Siga, 525-8577, Japan

ABSTRACT: Caseins form heterogeneous micelles composed of three types of disordered protein chains (α, β, κ), which include protein-bound calcium phosphate particles. We probe the stability limits of the micelle by applying hydrostatic pressure. The resulting changes of the size distribution and the average molecular weight are recorded in situ with static and dynamic light scattering. Pressure induces irreversible dissociation of the micelles into monomers above a critical value depending on their size. The critical pressure increases with temperature, pH, and calcium concentration due to the interplay of hydrophobic and electrostatic interactions. The pressure transition curves are biphasic, reflecting the equilibrium of two micelle states with different stability, average size, entropy, and calcium bound. The fast process of pressure dissociation is used to probe the slow equilibrium of the two micelle states under various conditions. Binding and release of β-casein from the micelle is suggested as the molecular mechanism of stabilization associated with the two states. In situ FTIR spectroscopy covering the P−O stretching region indicates that bound calcium phosphate particles are released from serine phosphate residues at pressures above 100 MPa. The resulting imbalance of charge triggers the complete decomposition of the micelle.

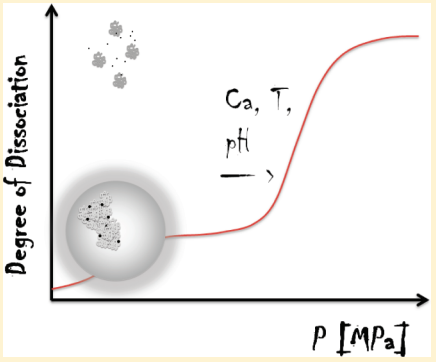

INTRODUCTION

Casein micelles, a major constituent of milk, are highly polydisperse molecular assemblies with a mean hydrodynamic size near $d_H \approx 150$ nm. Their main physiological task is to provide soluble calcium phosphate to the neonates: About 1 mM casein in milk binds 20 mM calcium and 10 mM phosphate, while the solubility of Ca_2PO_4 in aqueous solution is only 10^{-6} M. Precipitation of calcium is prohibited by formation of colloidal particles with a protein coat. In contrast to conventional surfactant micelles, casein is a proteinaceous heteropolymer, composed of four disordered peptide chains, α_{S1}-, α_{S2}-, β-, and κ-casein.[1] Their primary structure shows distinct hydrophilic and hydrophobic regions, which are at the focus of the dual binding model of stabilizing interactions in caseins.[2,3] The hydrophilic regions in α_{S1}-, α_{S2}-, and β-casein are rich in phospo-serines, which bind micelle calcium phosphate (MCP). The binding neutralizes the negative charge of phosphor-serine, stabilizing the micelle.

Hydrostatic pressure causes the irreversible dissociation of the micelle into smaller fragments, as previously observed by light scattering and turbidity experiments[4−6] and imaging techniques such as electron microscopy[7,8] and atomic force microscopy.[9,10] Combining dynamic light scattering and AFM, we have recently studied the size distribution of pressure decomposed casein micelles.[10] Up to 240 MPa small fragments with 20 nm size are observed, while at 300 MPa the dissociation into monomeric constituents is completed. For pressures above 300 MPa and the release to ambient pressure, the reassociation into mini-micelles of 25 nm in size is observed. Dissociation reactions, studied versus the temperature, pH, and Ca-concentration, allow one to sort out the various contributions to micelle stability as will be shown below in detail.[6,11]

Pressure is the relevant thermodynamic variable to separate volume-dependent effects from those of entropy or charge.[27] The specific volume of protein oligomers and other biomolecular assemblies generally exceeds the combined volume of its monomer constituents. The application of pressure thus destabilizes molecular complexes. Dissociation occurs at a critical value, when the chemical potential of the complex, $\Delta\mu_{ass}$, turns positive, depending on the positive association volume, $\Delta V_{ass} > 0$, and the chemical potential difference relative to the monomer state at ambient pressure $\Delta\mu_0$:

$$\Delta\mu_{ass}(P,T) = \Delta\mu_0(T, \mathrm{pH}, c_{Ca}) + P\Delta V_{ass} \qquad (1)$$

If the pressure-induced dissociation reaction is reversible, one can deduce from the two-state transition curve both ΔV_{ass} and the stabilization free energy $\Delta\mu_0$. In many applications of

Received: August 12, 2010
Revised: December 14, 2010

   dx.doi.org/10.1021/jp107622d | J. Phys. Chem. B XXXX, XXX, 000–000

practical interest, however, pressure-induced dissociation is neither two-state nor reversible. This is the case with casein dissociation, due to the slow precipitation of released calcium phosphate.

In the following, we show that fast pressure dissociation can be used to probe a slow conformational equilibrium and the resulting changes in stability versus the temperature, pH, and Ca-concentration. The dissociation process and the size distribution is monitored by light scattering, while the dissociation of colloidal calcium is recorded with high-pressure FTIR in the P−O stretching region.

Association−dissociation reactions of macromolecular assemblies were investigated before using pressure with a variety of scattering techniques, elastic X-ray and neutron scattering (SAS),[12−14] quasi-elastic neutron scattering,[15−17] light scattering,[10,18,19] and Raman scattering.[20,21] Fourier transform infrared spectroscopy (FT-IR) in combination with a diamond pressure cell has been mainly used to detect pressure-induced structural changes in the secondary structure of proteins.[22−26] The specific goal of our study is to probe the molecular interactions in casein micelles using a combination of high pressure and light scattering.

MATERIALS AND METHODS

1. Sample Preparation. Casein micelles from commercial-grade skim milk were extracted by combined uniform trans-membrane pressure micro-filtration (mean pore diameter, 0.1 μm) and ultra-filtration, concentrated by five washing steps and drying in a spraying tower.[28] Casein powder was dissolved in a filtered 0.1 M MES/Tris-HCl buffer, which is pressure-insensitive with respect to changes in pH, at a concentration of 40 mg/mL. The pH was adjusted by mixing different volumes of the buffer components. Different amounts of $CaCl_2$ salt were added to the buffer solution for the calcium-dependent measurements with concentrations ranging from 0 to 100 mM. All solutions were equilibrated by thoroughly stirring for 5 h. Within the recorded range, the properties of the sample were reversible with respect to changes in temperature, calcium concentration, and pH.

2. Light Scattering Experiments. To characterize the samples, angle-dependent light scattering experiments at ambient pressure were performed using an ALV DLS-goniometer system (ALV Laser GmbH, Langen, Germany). Static and dynamic light scattering experiments at different hydrostatic pressures were performed using the ALV-NIBS System (ALV-Laser GmbH, Langen) equipped with a SITEC high-pressure optical cell with four sapphire windows. For the turbid samples, the light of a 10 mW He−Ne laser (λ = 632.8 nm) was focused on the surface of the sample inside the pressure cell. The back-scattered light was recorded in a 177° back-scattering geometry using a sensitive avalanche diode detector. The resulting signal was transmitted to a multiple time scale correlator (ALV). The optical setup was tested with the requirement that the resulting size distribution of the turbid sample was nearly identical to the one determined from the same sample, which was diluted and thus transparent. The back-scattering technique minimizes the effects of multiple scattering, which corrupts the information on single molecule properties. The single scattering intensity of light $I(\theta, d_i)$ of a sample of noninteracting particles with diameter d_i at angle θ is proportional to the concentration $c_i(P)$ of species "i" at pressure P and the square of the molecular weight M_i^2.[39] The scattering

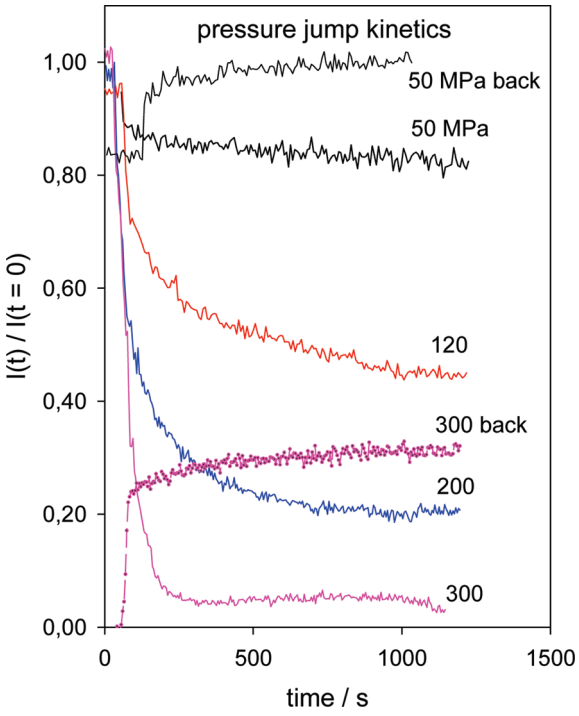

Figure 1. Time-dependent light scattering intensity (normalized to ambient pressure) after a pressure jump reflecting the dissociation or association of casein micelles (50 mM). The magnitude of the pressure jump (up or down) is indicated. The light scattering signal assumes a transient plateau, which decreases with pressure, after approximately 1200 s. The initial signal is recovered after pressure release from 50 MPa. Only partial recovery of the intensity occurs after release to ambient pressure from 300 MPa (back).[10,11]

intensity at various pressures was normalized to the value observed at ambient pressure (P = 0):

$$\frac{I(\Theta,P)}{I(\Theta,P=0)} = \frac{\sum_i P(Kd_i)\cdot c_i(P)\cdot M_i^2}{\sum_i P(Kd_i)\cdot c_i(P=0)\cdot M_i^2} \qquad (2)$$

The scattering vector K is given by $K = 4\pi\cdot\sin(\Theta/2)/\lambda$, Θ denotes the scattering angle, and λ is the wavelength of laser beam. The angle-dependent function $P(K\cdot d_i)$ includes the form factor of the particles with diameter d_i. It is unity for transparent solutions of particles with the diameter less than the wavelength of light. For a particle size below 300 nm at laser wavelength of λ = 632 nm, the angle dependence of the scattered intensity is small and was therefore neglected. The high turbidity of casein solutions arises from the high concentration of micelles (1 mM), which is enhanced by a small fraction of very large micelles (>300 nm). Dissociation of a single complex into N identical fragments increases the concentration of scattering centers by a factor N, but it decreases the molecular weight by the same factor. Together this leads to a reduction in relative intensity by a factor N according to eq 2. Such a two-state model of complex and monomer applies to casein, because the intact micelles ($d_H \approx$ 300 nm) disintegrate into small fragments below 30 nm in size.[10]

After a pressure jump, the light scattering signal decreases in time due to the dissociation of casein micelles, which is displayed in Figure 1 for various final pressures. The signal assumes a transient plateau at about 1200 s, which decreases with increase in pressure up to 400 MPa, where the dissociation is rather

dx.doi.org/10.1021/jp107622d |J. Phys. Chem. B XXXX, XXX, 000–000

complete. The signal recovers completely after pressure release from below 100 MPa (Figure 1). After release from higher pressures, only a partial reassociation is observed. Previously, we have reported detailed pressure-induced kinetics together with the structure of the resulting intermediates combining in situ light scattering and ex situ AFM.[9] On the basis of this information, we approximate the light scattering signal by assuming two states, micelle and monomers. We then define a degree of dissociation $f_{diss}(P)$ from the light scattering intensity $I(P,t)$. The intensity is evaluated in the plateau region at 1200 s after the pressure jump. Because fragments yield only a small contribution to the signal, a time-independent background scattering due to the fragments at 400 MPa (<10%) is subtracted from the signal. In the following, we use this operational definition of the dissociated fraction $f_{diss}(P)$ to probe temperature, pH, and Ca-dependent equilibrium of casein micelle structures:

$$f_{diss} = 1 - \{I(P, t = 1200\ s) - I(P = 400\ \text{MPa})\}/$$
$$\{I(P = 0.1\ \text{MPa}) - I(P = 400\ \text{MPa})\} \quad (3)$$

With dynamic light scattering, one evaluates the correlation function of scattered electric field $g^1(t,K)$ of thermal fluctuations induced by macromolecular diffusion. Multiple exponential decays are analyzed in terms of a cumulant expansion:[39]

$$\ln[g^1(t,K)] \approx -K_1 t + K_2 t^2 - 1/6 K_3 t^3 + \ldots \quad (4)$$

The first cumulant of $g^1(t,K)$ of a polydisperse solution of macromolecules yields the z-average diffusion coefficient from $K_1 = K^2\langle D\rangle_Z$. For a distribution of small compact particles with concentration $c_i(P)$ at pressure P for each species and diffusion coefficient D_i, one obtains:[39]

$$\langle D\rangle_Z = \frac{\sum_i c_i \cdot M_i^2 \cdot D_i}{\sum_i c_i \cdot M_i^2} = \frac{k_B T}{3\pi\eta\langle d_H\rangle_Z} \quad (5)$$

Assuming Stokes law for equivalent spheres, it is possible to calculate the average diameter of the equivalent hydrodynamic sphere $\langle d_H\rangle_Z$. k_B is the Boltzmann constant, T is the temperature in K, and η denotes the solvent viscosity. d_H is evaluated with the viscosity corrected for pressure effects according to ref 29. With the higher cumulants in eq 4, one can approximately reconstruct the radius number distribution. This was done using the ALV-provided program CONTIN, which calculates an approximate Laplace transform of the electric field correlation function.[39]

3. High-Pressure FTIR Spectroscopy. Infrared experiments with casein dissolved in D_2O (to avoid the strong O−H stretching absorption band) were performed using a Bruker Equinox 55 FTIR spectrometer equipped with a liquid-nitrogen cooled MCT detector and a thermo-stated diamond anvil cell (Diacell Products Ltd.). A stainless steel gasket with 2 mm diameter was inserted between the diamonds. The pressure was determined from the uncoupled O−H stretching frequency at 3400 cm^{-1}, where the peak frequency varies by −3.5 cm^{-1}/200 MPa.[30] The experiments were performed after the completion of hydrogen−deuterium exchange in the backbone amide protons, when no further change in the frequency region around 1550 cm^{-1} (amide II band) was detected. Additional information about the experimental setup and the preparation procedures is given in ref 23.

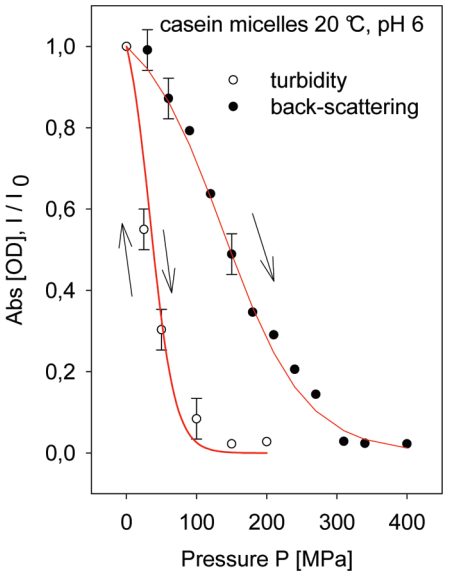

Figure 2. Turbidity (absorbance at 900 nm) of a 3% (w/v) casein solution at 20 °C, 10 mM calcium, pH 7.3, Tris-HCl (○); the "●" represent back-scattering intensity at 177° from the surface of the sample. Both data sets were normalized by their value at ambient pressure. The full lines represent fits of the data to eq 7. The parameters are given in the text. The arrows indicate the direction of the pressure change.

RESULTS

A. Light Scattering. *1. Pressure Effect on Molecular Weight and Radius Distribution of Casein Micelles.* Milk is an opaque liquid, which is the result of multiply scattered light from the concentrated solution of casein particles. The most striking effect of pressure application is a nearly transparent solution of clear milk. Figure 2 shows the turbidity transition of a concentrated casein solution by recording the transmission change of infrared light at 900 nm. The turbidity decreases rapidly with pressure, reaching a low level at 100 MPa. This is a clear sign of pressure-induced dissociation of casein particles. This process is fully reversible within a few hours.

Figure 2 also displays the single-scattering intensity versus pressure from back-scattering experiments taken at 1200 s after the pressure jump. The single-scattering intensity decreases more slowly with the pressure than the turbidity, reaching a low plateau around 300 MPa. The fractional change of this quantity reflects the decrease of the average molecular weight due to dissociation (eqs 2 and 3). The turbidity, which is dominated by multiple scattering, is more biased by the heavy particles of a distribution than single scattering. Their different pressure dependence thus points to a pronounced polydispersity in response to pressure: Larger micelles appear to be more susceptible to pressure dissociation than less massive particles. Moreover, the low level of the back-scattered intensity above 300 MPa implies that the molecular weight of the dissociation fragments is lower by at least a factor of 10 as compared to the intact micelles. From a previous study of pressure-dissociated casein micelles, it is known that this process leads to small fragments (<30 nm) at all pressures.[10]

For an initial analysis of the data in Figure 2, we thus assume a pressure-dependent equilibrium of just two conformations, M, intact micelles of monomers m: M ↔ m. It will turn out that

dx.doi.org/10.1021/jp107622d |J. Phys. Chem. B XXXX, XXX, 000–000

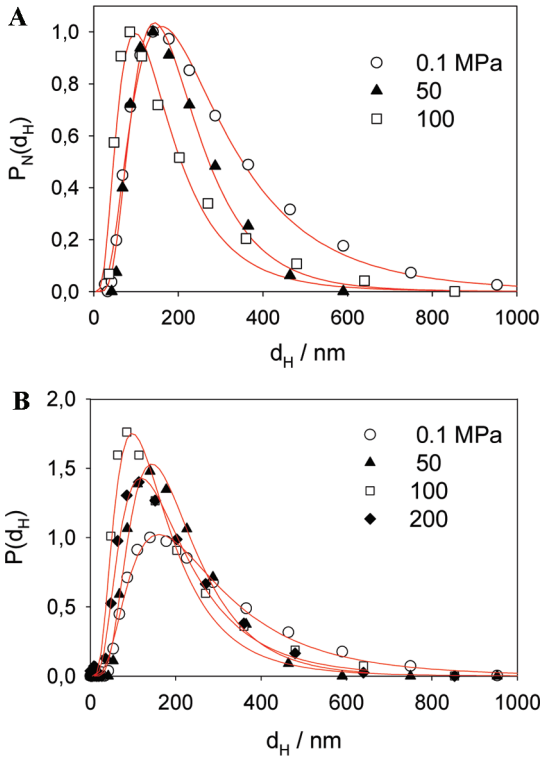

Figure 3. (A) Normalized size distribution $P_N(d_H)$ for intact micelles at low pressures and fits according to a log-normal distribution (eq 8). (B) Size distribution of intact micelles (undissociated fraction) versus pressure and fits to a log-normal distribution $P_{LN}(d_H)$ (eq 8), normalized to the area.

the double arrow implies "equilibrium" only at low pressures <100 MPa (Figure 1). At higher pressure, the dissociation M → m is not fully reversible. The small signal at high pressure (>300 MPa) indicates that the low molecular weight fraction "m" contributes only a negligible light scattering signal at all pressures.[10] We start with the analysis of low pressure equilibrium region: The difference in the chemical potential $\Delta\mu_{Mm}$ varies with pressure and temperature according to the Gibbs−Duhem relation relative to a reference state P_0, T_0:

$$\Delta\mu_{Mm} = \Delta\mu^0_{Mm}(P_0, T_0) + \Delta V_{Mm}\cdot(P - P_0) - \Delta S_{Mm}\cdot(T - T_0) \quad (6)$$

ΔV_{Mm} and ΔS_{Mm} denote the respective difference in volume and entropy between the micelle and the monomer solution. The mass fraction of intact and dissociated micelles is denoted by f_M, and $f_m = f_{diss}$ and $f_M + f_m = 1$. The equilibrium fraction of dissociated micelles versus pressure at fixed temperature is then calculated from:[27]

$$f_{diss} = 1 - \frac{1}{1 + \exp\left(\frac{1}{RT}(-\Delta\mu^0_{Mm} - (P - P_0)\cdot\Delta V_{Mm})\right)} \quad (7)$$

The width of the pressure-induced dissociation curve depends on the magnitude of the transition volume $\Delta V_{ass} = \Delta V_{Mm}$. For the turbidity transition in Figure 2, one derives from eq 7 a stabilization free energy of $\Delta\mu^0_{Mm} = -5$ (±1) kJ/mol and a transition volume of $\Delta V_{Mm} = 140$ (±10) ml/mol. ΔV_{Mm} thus corresponds to a volume of about eight water molecules (18 mL/mol), which appears reasonable for a complex of this size (300 nm). In view of the reversibility of the transition at low pressures, the two-state equilibrium model may be a reasonable approximation despite the polydispersity. By contrast, the dissociation transition recorded with the back-scattering method is much broader and yields a correspondingly smaller transition volume of $\Delta V_{ass} = 42$ (±5) ml/mol. Such a low value is typically observed for the unfolding of small (3 nm) globular proteins, which seems implausible for 300 nm particles. Moreover, the pressure-induced dissociation process is not fully reversible, as shown in Figure 1 and elsewhere.[10,11] This suggests that the width of the transition, recorded by back-scattering in Figure 2, is enhanced by the polydispersity of the solution, leading to a small apparent transition volume. The micelle stability should thus vary with size and molecular weight. To test this idea, we measured the pressure-dependent size distribution using dynamic light scattering experiments. The respective intensity correlation functions are not exponential in time, reflecting the heterogeneity in micelle size. In Figure 3A, we display a normalized size distribution of casein micelles $P_N(d_H)$ at three pressures across the range, where turbidity transition occurs. At ambient pressures, the data reproduce the well-known polydispersity of casein micelle solutions, yielding an average diameter d_H of 305 nm. Its shape is well approximated by a log-normal distribution, $P_{LN}(d_H)$ (Figure 3A), which is consistent with a previous analysis reported by de Kruif.[31] Figure 3A and B also demonstrates that a log-normal distribution is a good choice for the undissociated fraction above ambient pressure:

$$P_{LN}(d_H) = \frac{1}{\sqrt{2\pi}\sigma_d d_H}\exp\left[-\frac{(\ln(d_H/d_0))^2}{2\sigma_d^2}\right] \quad (8)$$

The respective parameters vary with the pressure. d_0 is the most probable diameter, and σ_d denotes its standard deviation. Table 1 lists the corresponding values, the averages size, and the spread from the fits to the distributions of Figure 3B. The application of pressure reduces the average diameter from 300 to 200 nm, and the spread decreases from 220 to 125 nm. The distribution, however, shrinks from the large size end (Figure 3A). This implies that large micelles decompose at lower pressures and are thus less stable than small micelles. The distribution shrinks with pressure predominantly due to dissociation of large micelles. However, this trend is reversed above 200 MPa. Both radius and variance, which refer to the undissociated fraction at a 20% level, increase again. Thus, at higher pressures, preferentially micelles with diameters below the optimal value decompose. This result can be explained by a stability optimum at an intermediate size d_0, compatible with a pronounced maximum of the size distribution. The logic behind the log-normal size distribution is most likely a Gaussian distribution of stabilization free energies, $\Delta\mu_0$, about a maximum

Table 1. Properties of the Log-Normal Size Distribution (Figure 3B)

P [MPa]	σ_d	d_0 [nm]	$\langle d_H\rangle$ [nm]	$(\langle\Delta d^2\rangle)^{1/2}$ [nm]
0.1	0.65	245	305	220
50	0.63	190	220	125
100	0.63	148	180	125
200	0.64	181	224	160

dx.doi.org/10.1021/jp107622d |J. Phys. Chem. B XXXX, XXX, 000–000

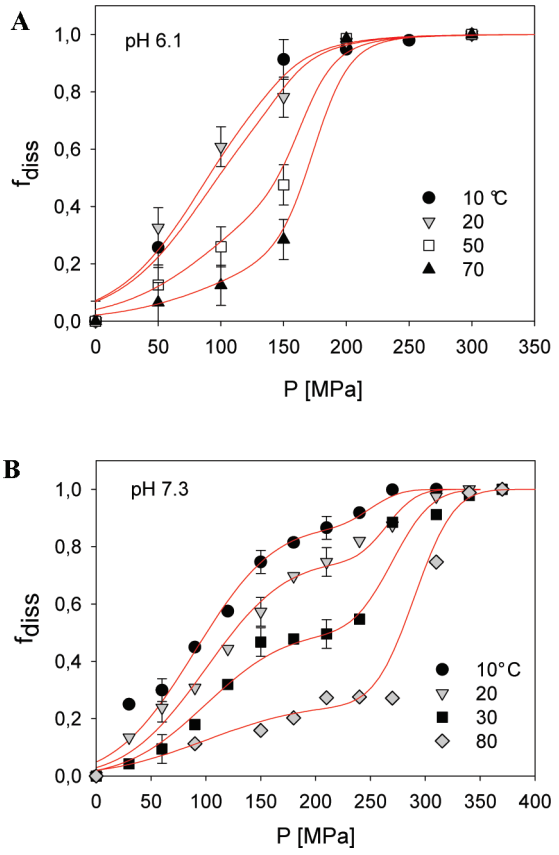

Figure 4. (A) Dissociated fraction of casein micelles versus pressure at pH 6 from back-scattering according to eq 3 and fits according to the two-component model of eqs 10−12. (B) Dissociated fraction of casein micelles versus pressure as in Figure 4A at pH 7.3 and fits to the two-component model.

stability $\Delta\mu_{max}$ according to $(\Delta\mu_0 - \Delta\mu_{max})/RT \propto \log(d_H/d_0)$:

$$P_G(\Delta\mu_0) = \frac{1}{\sqrt{2\pi}\sigma} \exp\left[-\frac{(\Delta\mu_0 - \Delta\mu_{max})^2}{2\sigma^2}\right] \qquad (9)$$

This distribution is shown in Figure 9B with parameters taken from the reversible turbidity transition in Figure 2. The pressure increase enhances the free energy of the micelles according to $d\mu = V\,dP$. If the dissociated state has the lower volume, then an increase in pressure will destabilize the micelle with respect to the monomer state. For any particular size d_i of micelle i, there exists a critical pressure $P_i(d_i)$, where $\Delta\mu_{Mm}(d_i,P_i) = 0$; at higher pressure, the micelle will decompose to monomers. By pressure dissociation, it is thus possible to probe the distribution of stabilization free energies of the micelles. This concept will be expanded in the next section.

2. Pressure Dissociation as a Probe of the Temperature-Dependent Stability of Casein Micelles. The average back-scattering intensity varies with the average molecular weight of the distribution according to eq 2. For the average dissociation behavior versus pressure, as discussed above, only two classes of states have to be taken into account, the intact micelles "M" and the small fragments "m". The normalized back-scattering intensity is thus a direct measure of the degree of dissociation f_{diss}, as

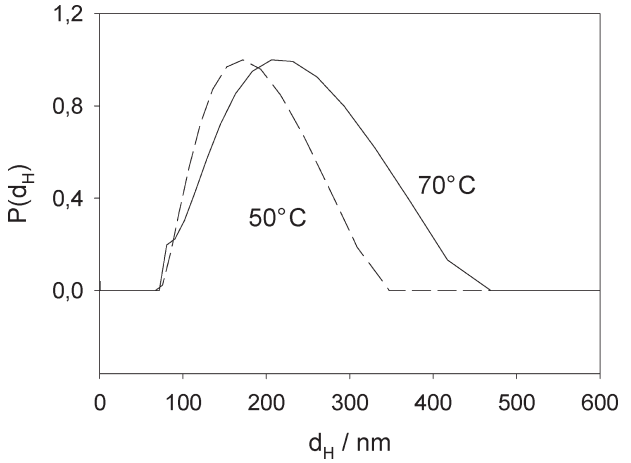

Figure 5. Size distribution of casein micelles (40 mg/mL) at low Ca-concentration (10 mM, pH 6.1) at ambient pressure at 50 and 70 °C.

defined by eq 3. The effect of pressure and temperature on the degree of dissociation f_{diss} of a casein solution at pH 6.1 is shown in Figure 4A. Thus, an increasing fraction of micelles becomes destabilized above 50 MPa. No micelles can exist beyond 300 MPa. A midpoint of the dissociation transition $P_{1/2}$ can be defined by $f_{diss}(P_{1/2}) = 0.5$. $P_{1/2}$ shifts from 100 MPa at 10 °C to 170 MPa at 70 °C. The average stability of the micelles thus increases with the temperature. Analogous experiments, performed at pH 7.3 in Figure 4B, display the same stabilizing effect, but now the transition curve reveals two well-resolved steps. The respective midpoints of the two-level transition at $P_{1/2} = 100$ and 250 MPa appear to be independent of the temperature. However, the relative amplitude of the two steps varies with the temperature; the second step is more prominent at higher temperature. This result suggests that two subpopulations within the distribution of micelles with different stability exist. Moreover, the transition does not depend on the history of temperature changes. This result is compatible with a slow conformational equilibrium between two micelle substates, $M_1 \leftrightarrow M_2$, which shifts from M_1 to M_2 with increasing temperature. Because pressure dissociation is fast as compared to the slow $M_1 \leftrightarrow M_2$ equilibrium, it is possible to probe the population of the two undissociated micelle states, as it varies with the temperature. The respective kinetic model is displayed in Figure 9. The brackets enclosing $\{M_1\}_i$ and $\{M_2\}_i$ symbolize the heterogeneous ensemble of micelles in each state differing in size (i). The $P_1(i)$ and $P_2(i)$ denote the dissociation pressures of the two states as they vary with size (i). A preliminary report of the temperature effect on micelle stability was published in ref 11. The gain in pressure stability is accompanied by an upshift in the average micelle size when the temperature increases from 50 to 70 °C, as shown in Figure 5. One feature of the M_2 population, distinguishing it from M_1, seems to be a larger average micelle size.

By contrast, this gain in stability in parallel with a larger average size should be distinguished from the preferential dissociation of larger micelles with pressure in a given distribution displayed in Figure 3A.

3. Pressure Dissociation as a Probe of Ca-Dependent Stability of Casein Micelles. We now keep the temperature fixed at a low value (20 °C, pH 7.3) and probe the effect of calcium concentration on the pressure dissociation curves. Figure 6A displays two well-resolved dissociation transitions, which

dx.doi.org/10.1021/jp107622d |J. Phys. Chem. B XXXX, XXX, 000–000

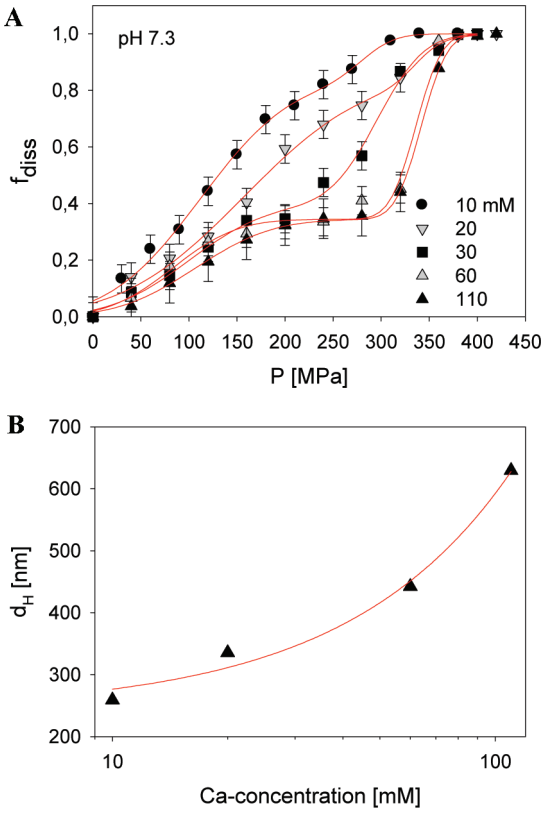

Figure 6. (A) Dissociated fraction of casein micelles at 20 °C, pH 7.3 versus pressure at various concentrations of calcium and fits (Table 3) according to the cumulative dissociation model, eqs 10−12. (B) Average hydrodynamic diameter d_H of casein micelles versus calcium concentration.

become more pronounced at higher concentration. The transition curves in Figure 6A resemble the data displayed in Figure 4B, where the temperature was varied at low Ca-concentration. In contrast to the fixed position of the first transition at about $P_{1/2}$ = 120 MPa, the midpoint of the second step shifts to higher pressures with increasing calcium-concentration. Moreover, the M_1 dissociation amplitude is diminished, while the magnitude of the second transition, the dissociation of M_2, increases accordingly. The maximum amplitude of M_2 is observed at calcium concentrations between 60 and 100 mM. No further enhancement occurs above 100 mM. For calcium concentrations exceeding 110 mM, association and precipitation of casein at ambient pressures is observed. This behavior is consistent with the increase of the average hydrodynamic radius observed at high calcium concentrations (Figure 6B).

4. Synergistic Effects of Temperature and Calcium Concentration on the Stability of Casein Micelles. The combined effect of temperature and calcium concentration on the pressure stability of casein micelles is displayed in Figure 7. A single dissociation transition of M_1 occurs at low temperature and low calcium concentration as well as at high temperature and high concentrations. The respective $P_{1/2}$ values are quite different, however. At intermediate T and c_{Ca}, a two-step dissociation occurs, either at high temperatures and low concentration or alternatively at high calcium concentration and low temperatures. The respective dissociation curves $f_{diss}(P)$ are different, however. For instance, in the presence of 60 mM calcium at 80 °C, there is no change of the degree of dissociation up to 300

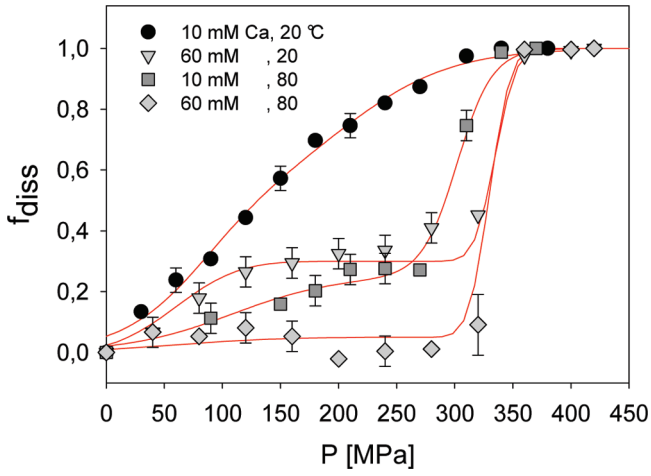

Figure 7. Dissociated fraction of casein micelles versus pressure at various combinations of temperature and calcium concentration and fits according to the cumulative dissociation model, eqs 10−12.

MPa. At higher pressures, a sharp dissociation transition occurs. From the width of the transition, one estimates a dissociation volume of ΔV_{ass} = 160 mL/mol as a lower limit. This is compatible with ΔV_{ass} = 140 mL/mol, derived from the turbidity transition. Enhanced temperature and Ca-concentration further increase the pressure stability: At 80 °C and 60 mM calcium, the transition pressure value is $P_{1/2}$ = 320 MPa, as compared to $P_{1/2}$ = 300 MPa at 20 °C and 60 mM calcium, and $P_{1/2}$ = 280 MPa at 80 °C without calcium.

In the intermediate range up to 250 MPa, the micelles are more stable in the presence of 10 mM calcium and 60 °C than those at 20 °C and 110 mM calcium. Calcium concentration and temperature are thus synergistic variables. This result indicates that native micelles are stabilized by two types of interactions, electrostatic and hydrophobic forces, which can be varied independently. Moreover, the equilibrium of the two discrete conformations can be shifted independently from M_1 to M_2 by increasing either the temperature or the calcium concentration.

5. Effect of pH on Pressure Stability of Casein Micelles. As shown in Figure 8A, native-like casein micelle preparations at low Ca-concentrations (10 mM) show a single dissociation step at $P_{1/2}$ = 120 MPa and exhibit no pH dependence from pH 6.1 to 8.1 in their pressure stability. To the contrary, a pronounced two-step behavior emerges at intermediate Ca-concentrations (60 mM) as shown in Figure 8B. $P_{1/2}$ increases with pH from 224 MPa at pH 6.1 to 400 MPa at pH 8.1. Most interesting, only the second step, and thus the stability of conformation M_2 changes with pH, while conformation M_1 is not affected. This suggests that M_2 is stabilized both by electrostatic and by hydrophobic interactions, while hydrophobic contacts dominate in M_1.

6. Data Analysis. In this section, we introduce a model to derive approximate molecular information from the observed pressure dissociation curves. In the ideal case of a pressure-dependent equilibrium between two states of monodisperse molecules, the free energy difference and the transition volume can be easily extracted. The energy difference and the transition volume together fix the midpoint of the transition on the pressure scale according to $\Delta\mu_0 = -P_{1/2}\Delta V_{ass}$. The transition volume is proportional to the slope of the transition curve at $P = P_{1/2}$, that is, $(df_{diss}/dP)|_{P1/2} = \Delta V_{ass}/(4RT)$. With casein micelles, this

dx.doi.org/10.1021/jp107622d |J. Phys. Chem. B XXXX, XXX, 000–000

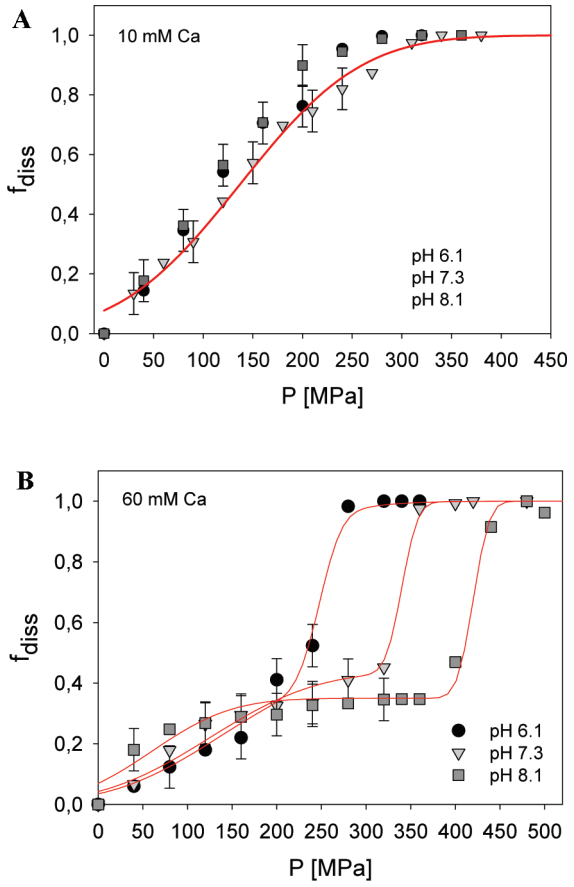

Figure 8. (A) Dissociated fraction of casein micelles versus pressure and pH (symbols in B) at low calcium concentration (10 mM) and fit (line) according to the cumulative dissociation model, eqs 10−12. (B) Dissociated fraction of casein micelles versus pressure and pH at high calcium concentration (60 mM) and fit (line) according to the cumulative dissociation model, eqs 10−12.

scenario is approximately fulfilled at low pressures, below 100 MPa, where we deduce from the turbidity change in Figure 2 a transition volume of 140 (±20) mL/mol. The same number also follows as the lower limit of ΔV_{ass} from the sharp second dissociation transitions in Figures 4B, 6A, and 8B, which are not fully reversible. We then assume $\Delta V_{ass} \geq 140$ mL/mol to convert the pressure to an energy scale according to $\Delta\mu_0 < -P\Delta V_{ass}$. This gives an upper bound to the stabilization free energy. Although the dissociation process is generally irreversible and the width of the transition curves is dominated by the heterogeneity of the micelle size, there are prominent equilibrium features revealed by the experiments: The dissociation transition versus pressure occurs in two steps, which is attributed to two species of micelles, which differ in stability. The corresponding mass fractions vary reversibly with the temperature, Ca-concentration, and pH. The slow equilibrium of the reversible states M_1, M_2 is probed by fast irreversible dissociation at the pressures $P_1(i)$ and $P_2(i)$, which vary with size i. The respective kinetic scheme is displayed in Figure 9A. For the pressure dissociation curves, only the average of $\{M_1\}_i$ and $\{M_2\}_i$ with respect to the size distribution (i) of the micelles is taken into account.

The mass fractions of the two i-averaged species M_1 and M_2 are determined from the respective amplitudes f_1 and f_2 of the two-step dissociation process. Here, any model yielding a sigmoid transition curve $S(P)$ is appropriate:

$$f_{diss} = f_1 \cdot S_1(P, P_{01}, \sigma_{P1}) + f_2 \cdot S_2(P, P_{02}, \sigma_{P2}) \qquad (10)$$

$P_{01} = P_{1/2}(1)$, $P_{02} = P_{1/2}(2)$, σ_{P1}, and σ_{P2} are the half-pressures and the width parameters of the two components, respectively. The resulting thermodynamic parameters are derived from f_1 and f_2 only and are largely independent of the peculiar choice of S_1 and S_2. Our specific choice of the S-functions is motivated by two basic properties of the casein system, polydispersity and irreversible pressure dissociation. The results of Figure 3 characterize the polydispersity via the size distribution: It is striking that the micelle size follows approximately a log-normal distribution. Applying pressure leads to dissociation primarily of the large size tail of the distribution. Size is thus a discriminating factor controlling micelle stability. It seems plausible that the log-normal distribution originates from a normal distribution of micelle stabilities according to eqs 8 and 9.

The dissociated fraction $f_{diss}(P)$ follows from cumulating a Gaussian distribution of micelle stability of species i, whose chemical potential is positive with respect to the dissociated state at pressure P:

$$\Delta\mu_i = \Delta\mu_{i0} + P\Delta V_i > 0 \qquad (11)$$

The dissociated fraction versus P is thus given by a cumulative Gaussian function versus pressure assuming a continuous distribution of species i:

$$f_{diss}(P) = \int_0^P dP \frac{1}{\sqrt{2\pi}\sigma_P} \exp\left(-\frac{(P-P_0)^2}{2\sigma_P^2}\right)$$
$$= 1 - 0.5\left(1 - \mathrm{erf}\left(\frac{P-P_0}{\sqrt{2}\sigma_P}\right)\right) \qquad (12)$$

where erf(x) denotes the error function and P_0 is the critical pressure characterizing the maximum of the distribution $\Delta\mu_0 = -P_0\Delta V_{ass}$, and σ_P is the width parameter. The dissociated fraction at a pressure P is interpreted as the result of a cumulative Gaussian distribution, shown by the gray area in Figure 9B.

A fit to the dissociated fraction in Figure 4A at pH 6.1 and 10 °C, assuming a single transition, yields the following parameters: P_{01} = 90 MPa ($\Delta\mu_0$ = −12.6 kJ/mol) and σ_{P1} = 60 MPa (8.4 kJ/mol). At 70 °C, these parameters are P_{02} = 175 MPa (−24.5 kJ/mol) and σ_{P2} = 35 MPa (4.9 kJ/mol). Alternatively, the same data can be adjusted at all temperatures to a model with a temperature-dependent equilibrium between two distinct micelle states M_1 and M_2 according to eq 10. The latter differ in maximum stability pressure P_0 and the width σ of the distribution.

Figure 4B clearly shows two dissociation steps. The resulting parameters are P_{01} = 100 MPa (−14 kJ/mol), σ_{P1} = 80 MPa, P_{02} = 250 MPa (−35 kJ/mol), and σ_{P2} = 30 MPa. This suggests that the enhanced apparent pressure stability with increasing temperature is better explained by a population change of two components, which are intrinsically independent of the temperature. A two-step model can also be applied to the data obtained at pH 6.1. Table 2 lists the resulting fitting parameters of eqs 10, 12. Figure 10A shows the corresponding temperature-dependent fractions for the $M_1 \leftrightarrow M_2$ equilibrium at pH 6 and 7.3. The conformation M_1 is more stable at low pH and low temperature. The equilibrium parameters of Table 4 indicate that the high

dx.doi.org/10.1021/jp107622d |J. Phys. Chem. B XXXX, XXX, 000–000

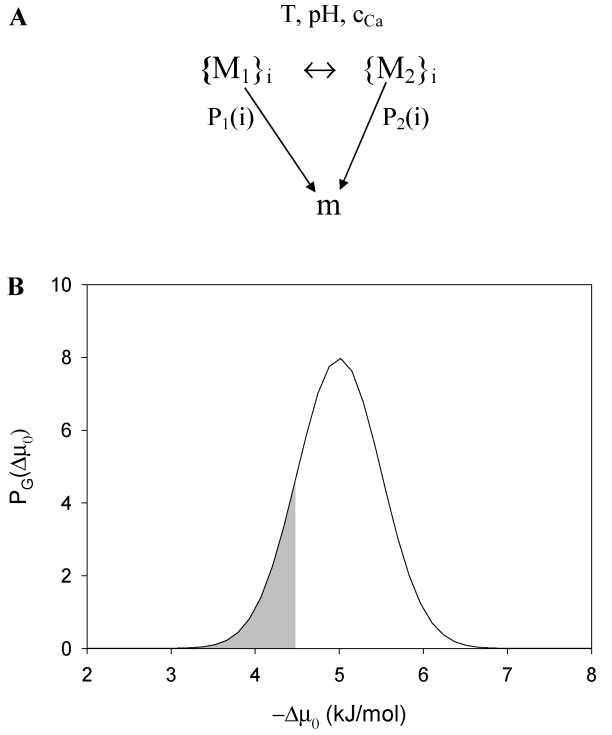

Figure 9. (A) Kinetic model to evaluate the fractions f_1 and f_2 from the pressure dissociation curves quantitatively. The slow equilibrium of the reversible states $\{M_1\}_i$ and $\{M_2\}_i$ is probed by fast irreversible pressure dissociation, resulting in small monomer fragments m. The subscript "*i*" indicates that each M-state is composed of a distribution of micelles (*i*) with different size. The two states exhibit different pressure stabilities and dissociate at $P_1(i)$ and $P_2(i)$, depending on the micelle size *i*. This heterogeneity determines the finite width of the transition. (B) Gaussian distribution of stabilization free energies according to eq 9, and the parameters of the reversible turbidity transition in Figure 2. Gray area: Dissociated fraction $f_{diss}(P)$ (gray area), fulfilling the condition of eq 11 at a particular pressure, which is the cumulative Gaussian distribution of stabilization free energy $\Delta\mu_0 \approx P$ according to eq 12.

Table 2. Fit Parameters for the Data in Figure 4 Derived from Eqs 10−12

T [°C]	f_1	P_{01} [MPa]	σ_1 [MPa]	f_2	P_{02}	σ_2
			pH 6			
10	1	89	83	0		
20	0.92	96	83	0.08	164	35
50	0.48	89	83	0.52	174	33
70	0.24	89	83	0.76	174	33
			pH 7.3			
10	0.85	90	80	0.15	240	30
20	0.75	100	80	0.25	265	30
30	0.5	110	80	0.5	282	30
40	0.5	100	120	0.5	250	50
80	0.25	100	100	0.75	290	40

temperature conformation M_2 is stabilized by a larger entropy, while M_1 exhibits a lower chemical potential at ambient pressure. The thermodynamic parameters of the pressure-independent

Table 3. Fit Parameters for the Data of Figure 6A, Derived from Eqs 10−12; Fit Parameters of the Data of Figure 7, According to Eqs 10−12; and Fit Parameters of Figure 8, According to Eqs 10−12

c_{Ca} [mM]	f_1	P_{01} [MPa]	σ_1 [MPa]	f_2	P_{02}	σ_2	rel. error
			Figure 6A				
10	0.84	112	105	0.16	280	38	7×10^{-4}
20	0.84	157	140	0.16	336	30	
30	0.4	100	90	0.6	296	55	
60	0.35	100	80	0.65	335	30	
110	0.34	106	89	0.66	341	30	

c_{Ca} [mM]/T[°C]	f_1	P_{01} [MPa]	σ_1 [MPa]	f_2	P_{02}	σ_2	rel. error
			Figure 7				
10/20	0.8	106	100	0.2	272	40	4×10^{-4}
10/80	0.31	135	130	0.69	308	20	
60/20	0.3	60	60	0.7	335	20	
60/80	0.05	(60)		0.95	330	20	

pH	f_1	P_{01} [MPa]	σ_1 [MPa]	f_2	P_{02}	σ_2	rel. error
			Figure 8				
10 mM Ca							
6−8	1	140	137				10^{-4}
60 mM Ca							
6.1	0.45	137	136	0.55	248	30	10^{-4}
7.3	0.44	130	136	0.56	340	20	
8.1	0.35	60	100	0.65	420	20	

$M_1 \leftrightarrow M_2$ equilibrium should not be confused with the pseudothermodynamic parameters describing the stability of the micelle with respect to pressure dissociation. An interesting question is whether the shift in the equilibrium between the populations M_1 and M_2 also leads to changes in the size distribution. Figure 5 shows that the radius distribution at 70 °C is displaced to higher values as compared to the size at 50 °C. This shift in the size of intact micelles is reversible. We have seen above that the micelles of large size exhibit a lower stability toward pressure dissociation. Thus, one has to distinguish changes in size within a given distribution from changes of the average value. An increase in average size at constant shape of the distribution seems to indicate a stability increase. This is also true for the size−stability relationship as a function of the Ca-concentration in Figure 6B. The same two-step dissociation analysis has been performed with the data shown in Figure 6A at fixed temperature and versus Ca-concentration. Figure 10B displays the resulting fractions f_1, f_2 versus Ca-concentration. It is interesting that neither the stability of M_1 nor that of of M_2 vary with the Ca-concentration; instead, only the population of the more stable conformation M_2 increases. This result indicates a coupled equilibrium between two structural conformations M_1 and M_2 and Ca-binding, where Ca binds preferentially to conformation M_2.

The resulting combined equilibrium constant of the process is calculated from:

$$K_{Ca} = K_M(T) \exp\left(f_{Ca} \ln \frac{c_{Ca}}{c_{Ca}{}^0}\right) \qquad (13)$$

dx.doi.org/10.1021/jp107622d |*J. Phys. Chem. B* XXXX, XXX, 000–000

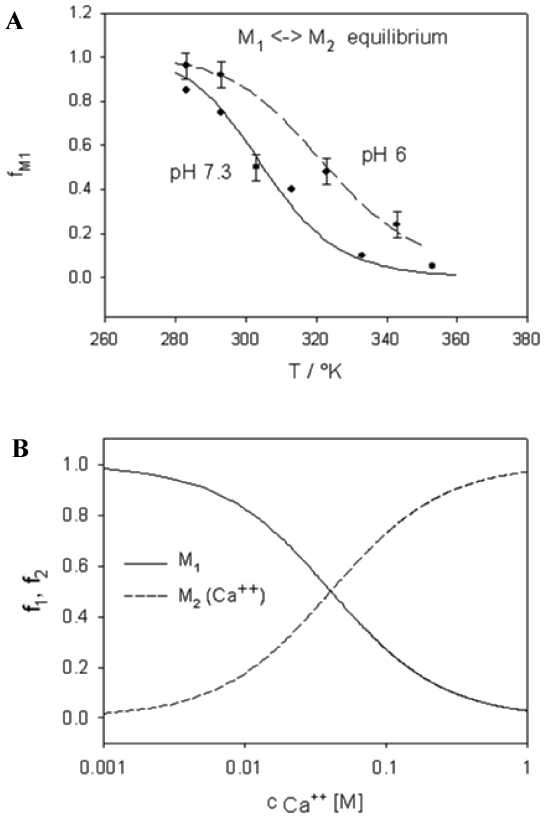

Figure 10. (A) Relative population of the "low temperature" state M_1 of the $M_1 \leftrightarrow M_2$ equilibrium at two pH values versus the temperature. The respective thermodynamic parameters are given in Table 4. (B) Variation of fractions f_1 and f_2 of the two casein micelle conformational states M_1 and M_2 derived from the pressure dissociation curves as a function of calcium concentration.

Table 4. Fit Parameters of Data in Figure 10A

pH	ΔH_{21} (kJ/mol)	ΔS_{21} (J/(mol·K)
6.1	60	200
7.3	73	240

$K_M(T)$ denotes the equilibrium constant of $M_1 \leftrightarrow M_2$ in the absence of calcium, and f_{Ca} is given by:

$$f_{Ca} = \frac{\beta \cdot c_{Ca}}{1 + \beta \cdot c_{Ca}} \qquad (14)$$

For the equilibrium constant at low Ca-concentration at 20 °C, we obtain $K_M = 0.18$, while for the Ca-binding constant, $\beta^{-1} = 40$ mM is deduced. Figure 10B shows the resulting population change of M_1 and M_2 versus the Ca-concentration. Equations 13 and 14 can also account for the synergistic stabilization of M_2 by increase of temperature and Ca-concentration as shown in Figure 7. At low Ca-concentration and temperature, only M_1 exists, which is not susceptible to pH changes. At intermediate and high Ca-concentration, however, a two-step transition occurs. In contrast to the effect of an increasing Ca-concentration (Figure 6A), the relative population of M_1, M_2 does not vary with pH. Instead, it is the midpoint of the second transition ($P_{1/2}$) that increases with pH. From the pH dependence of $P_{1/2}$ of M_2, one estimates that between one and two protons are being adsorbed during the dissociation process. This step becomes less likely with the lack of available protons, explaining why $P_{1/2}$ of M_2 increases with pH.

B. Release of Calcium Particles from Casein: High-Pressure FTIR Spectroscopy. Figure 11A compares the mid infrared spectrum of casein in the amide band region at two pressures, 0.1 and 320 MPa, where the micelles are either intact or fully dissociated. The absorption bands at 1642, 1569, and 1515 cm^{-1} arise from (1) the amide I vibration of the polypeptide backbone, (2) the $-COO^-$ asymmetric stretching vibration of Asp and Glu, and (3) the ring-stretching vibration the Tyr residues, respectively. The amide I band contour of casein at ambient pressure shows the characteristic features of a random backbone conformation.[32] The minor changes observed in this band, when the pressure goes up to 320 MPa, are compatible with small volume adjustments. Any major structural change of the backbone conformation, while the casein micelle is split into fragments, can be excluded. Second, there is no increment in band intensity of the $-COO^-$ asymmetric stretching vibration up to 320 MPa. This result excludes any direct binding or release of calcium particles to Asp or Glu residues: The dissociation of Ca^{2+} would produce charged Asp and Glu residues, enhancing the stretching band intensity. (3) The ring-stretching band of Tyr displays a minor shift to higher frequency with pressure due to the slight density increase of the environment but not a major change. If the colloidal calcium binds predominantly to the phosphate groups of phospho-serine residues, it is of particular interest to investigate the respective P−O stretching vibration. Native casein does not exhibit a significant band arising from the $-PO_3^-$ symmetric stretch at ambient temperatures and pressure, as shown in Figure 11B, although the $-PO_3^-$ form predominates for the phosphor-serine residue at pD 7.1. In contrast, EDTA-treated casein displays a prominent band at 976 cm^{-1} under almost identical conditions. Because the symmetric P−O stretching vibration is very sensitive to bond length and bond order of the P−O moiety,[33] the missing band intensity with native casein suggests some kind of ligand bound to the serine-phosphate residues. As reported in ref 34, this ligand seems likely to be the colloidal calcium particles.

When $CaCl_2$ is added to EDTA-treated casein, one observes that the $-PO_3-$ symmetric stretching band broadens and slightly shifts to higher frequency. It is remarkable that the symmetric stretching band is still significant after adding a 15-fold excess of Ca^{2+} relative to casein in molar units. This result indicates that the presence of $CaCl_2$ alone cannot reproduce the interaction between the serine-phosphate residue and the colloidal calcium particles of native casein. The binding mode of Ca^{2+} to serine-phosphate residues may thus be different from colloidal calcium. Figure 11C shows the effect of pressure on the infrared bands of native casein for the $-PO^{3-}$ stretching vibration. Two bands at 990 and 977 cm^{-1} emerge cooperatively when the pressure increases. The absorption band at 990 cm^{-1} is assigned to the phosphate ion HPO_4^{2-}, and the 977 cm^{-1} band is assigned to the $-PO_3^{2-}$ moiety of the serine-phosphate residue. The appearance of the latter band indicates that CCP particles are released from the phosphate residues by pressure, resulting in an increased negative charge of the casein molecules. Moreover, the simultaneous appearance of the former band suggests that the CCP particle dissociates into Ca^{2+} and HPO_4^{2-} when released from the serine phosphate residues. The increments in these two band intensities occur in parallel to the dissociation of the micelles as

dx.doi.org/10.1021/jp107622d |J. Phys. Chem. B XXXX, XXX, 000–000

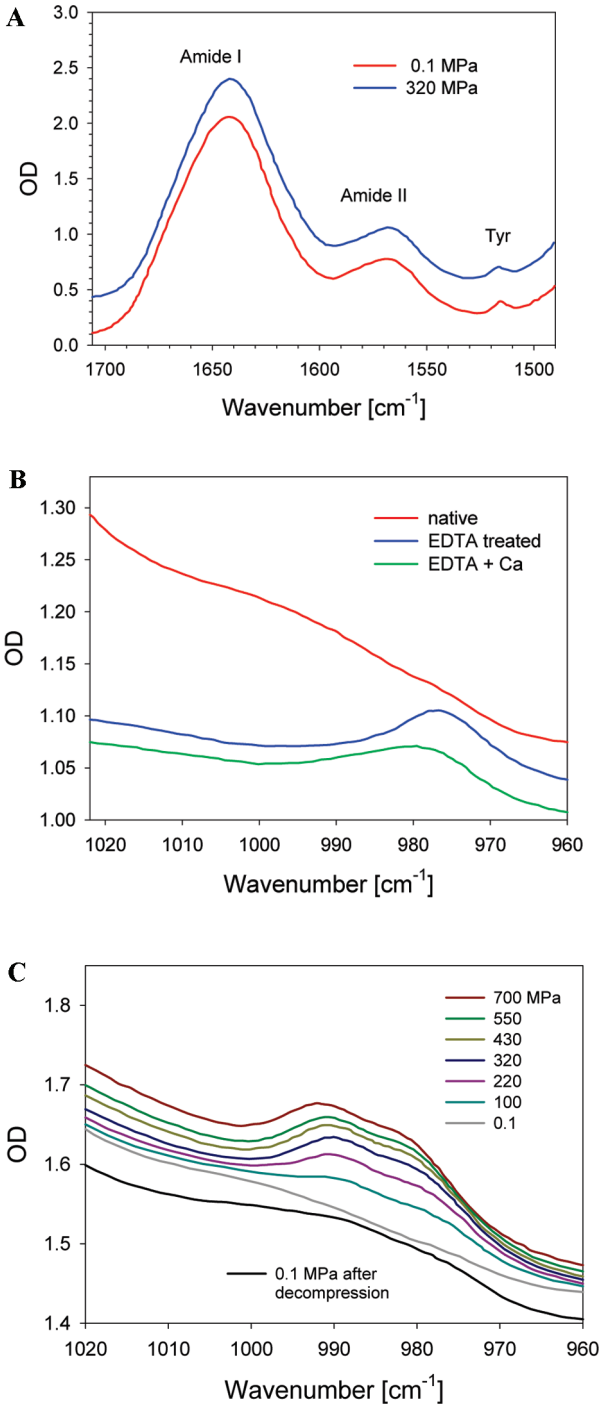

Figure 11. (A) Infrared spectra of native casein in D_2O (pD 7.1) and effect of pressure at 20 °C showing the amide I absorption band at 1640 cm^{-1}, the $-COO^-$ asymmetric stretch of Asp at 1565 cm^{-1}, and the tyrosin ring-stretching vibration at 1615 cm^{-1}. (B) Infrared absorption spectrum of the $-PO_3^{2-}$ symmetric stretching vibration of various caseins dissolved in D_2O at ambient temperature and pressure. Native casein (pD 7.1, red), EDTA-treated (pD 6.9, blue) casein, and casein with $CaCl_2$ added after EDTA treatment (pD 6.2, green) are shown. The concentrations of casein and $CaCl_2$ were 50 mg/mL and 30 mM, respectively. (C) Infrared spectra of native casein in D_2O (pD 7.1) in the $-PO_3^{2-}$ symmetric stretching region versus pressure and after pressure release. The spectrum after decompression is shown in black. The concentration of native casein was 50 mg/mL.

observed with light-back-scattering in Figure 1, which is complete at 300 MPa. This suggests that the dissociation of the whole casein micelle is related to the increment in negative charge of casein molecules under high pressure due to electrostatic repulsion. The spectrum after decompression still shows pronounced maxima due to phosphate ions, indicating that the dissociation of CCP particles is irreversible.

DISCUSSION AND CONCLUSION

The main goal of our study was to determine the various interactions, which stabilize the casein micelles under conditions close to native milk. This was done using the destabilizing action of pressure, by determining the critical pressure of the stability limit for the associated micelle. For the first time, we show that the stability decreases with increasing size of the heterogeneous distribution, and it increases with increasing temperature, pH, and calcium concentration. The pressure-induced transition curves are biphasic, suggesting two well-defined states with different properties. The relative population of these states varies with external conditions in a reversible manner. Our data can be consistently interpreted by assuming two discrete micelle states, M_1 and M_2, in equilibrium. M_2 is less populated than M_1 at ambient temperature due to a higher enthalpy, but it is more abundant at higher temperature because of its higher entropy (Table 4). Moreover, M_2 is more stable than M_1 at high pH and Ca-concentration, suggesting a lower electrostatic repulsion due to the binding of calcium to serine phosphate. Calcium thus binds preferentially to M_2, at high pH (Figure 8B), while the stability of M_1 is neither affected by pH nor by temperature changes (Figures 4 and 8A).

What is the molecular logic of two discrete states embedded in a continuous distribution of micelles of different size? One indication is provided by the average size, which increases in parallel with an enhanced stability (Figures 5 and 6B). The shape of the distribution, however, does change neither with increasing temperature nor calcium concentration. This observation is different and opposed to the narrowing and downshift of the size distribution in response to the application of pressure.

As a plausible mechanism of the stabilizing effect, we suggest the reversible association−dissociation equilibrium of a casein polypeptide with the micelle: Various experiments indicate that β-casein can dissociate reversibly from the micelle without causing complete disintegration. The $M_1 \leftrightarrow M_2$ equilibrium is thus tentatively identified with the binding of β-casein chains to the micelle:

$$\{M_1\}_i + \{\beta\text{-casein}\} \leftrightarrow \{M_2\}_i \qquad (15)$$

The brackets emphasize that eq 15 is not a stoichoimetric relation. Equation 15 explains qualitatively why the average micelle radius grows with increasing population of $\{M_2\}_i$ (Figures 5, 6B), because the association of β-casein with the micelles increases their size. By contrast, the narrowing of the size distribution with increasing pressure, which reflects the decomposition of predominantly large micelles, concerns the dissociation of all chains, α-, β-, and κ-casein. The association behavior of β-casein, a protein with distinct amphipathic character, has been studied in detail.[35] β-Casein in solutions below 10 °C is essentially a monomer. As the temperature increases to above 10 °C, micelles are formed by hydrophobic contacts. Also, electrostatic interactions are mediated by β-casein: At the natural pH of milk, pH 6.6, the hydrophilic N-terminal of β-casein is

dx.doi.org/10.1021/jp107622d |J. Phys. Chem. B XXXX, XXX, 000–000

highly charged, while the hydrophobic C-terminal has little if any charge. The α-caseins by contrast exhibit an association equilibrium, which depend very little on the temperature.[36] It is also well-known that the removal of calcium in subcritical amounts leads to a dissociation of weakly bound caseins from the micelle framework.[37,38] The framework is largely α-casein, while the dissociable proteins are mainly β-casein and κ-casein. The partially dissociated micelle at low calcium content and or low temperatures is thus likely the M_1 conformation, while M_2 corresponds to the native micelle with calcium and β-casein bound. The two-state model of M_1, M_2 should be considered as a first approximation. The β-casein−micelle equilibrium is as a multistep process, involving several molecules.[35]

The infrared spectra in the P−O stretching region show that Ca^{2+} is already 30% dissociated from the micelle at 100 MPa (Figure 11C). This suggests a coupled equilibrium between β-casein and Ca^{2+} binding to the micelle. The equilibrium constants for this process are given in section 6 in the context of eqs 13, 14. This information is derived from the population distribution of the slow $M_1 \leftrightarrow M_2$ equilibrium by fitting the pressure transition curves according to the model in Figure 9A. The qualitative conclusions concerning the change of the micelle stability with temperature, pH, and Ca-concentration together with the two-step nature of the dissociation transition are independent of such model assumptions. As explained above, the dissociation by pressure is not fully reversible above 100 MPa due to the formation of insoluble calcium phosphate. The resulting parameters associated with pressure dissociation are thus not true equilibrium values. We provide only lower limits to the equilibrium transition volume, $\Delta V_{ass} \geq 140$ mL/mol, and the associated (negative) free energy scale $\mu_0 < -P_{1/2}\Delta V_{ass}$.

To achieve these results, it was essential to perform in situ static and dynamic light scattering experiments at high pressures with turbid solutions at casein concentrations comparable with those of native milk. The variation in size of intact micelles follows a log-normal distribution at ambient and elevated pressures, suggesting a Gaussian distribution of stabilization free energies. Caseins form heterogeneous micelles, stabilized by a variety of interactions. Their understanding can facilitate the control of the aggregation of casein, which is an important aspect of milk product fabrication. Pressure-treated yogurt is commercially available in Japan. Future studies may address the role of the association−dissociation process of β-casein and its coupling to binding and release of calcium−phosphate particles. Incorporating a reversible calcium source into the reaction sequence will overcome the difficulties associated with irreversible pressure dissociation and will provide more accurate equilibrium constants.

AUTHOR INFORMATION

Corresponding Author

*Tel.: (+49) 8161 71 3536 (R.G.); (+49) 8122903562 (W.D.). Fax: (+49) 8161 71 4384. E-mail: ronald.gebhardt@wzw.tum.de (R.G.); wdoster@ph.tum.de (W.D.).

ACKNOWLEDGMENT

This work was supported by the Deutsche Forschungsgemeinschaft: Forschergruppe FR 456/25-4, project A1+A4. We thank J. Friedrich and A. Delgado for helpful suggestions and stimulating discussions.

REFERENCES

(1) Walstra, P.; Jenness. *Dairy Chemistry and Physics*; R. John Wiley and Sons: New York, 1984.
(2) Horne, D. S. *Int. Dairy J.* **1998**, *8*, 171.
(3) Horne, D. S. *Colloids Surf., A* **2003**, *213*, 255.
(4) Huppertz, T.; de Kruif, C. G. *J. Agric. Food Chem.* **2006**, *54*, 5903.
(5) Orlien, V.; Knudsen, J. C.; Colon, M.; Skibsted, L. H. *Food Chem.* **2006**, *98*, 513.
(6) Orlien, V.; Boserup, L.; Olsen, K. *J. Dairy Sci.* **2010**, *93*, 12.
(7) Needs, E. C.; Capellas, M.; Bland, A. P.; Manoj, P.; Macdougal, D.; Paul, G. *J. Dairy Res.* **2000**, *67*, 329.
(8) Knudsen, J. C.; Skibsted, L. H. *Food Chem.* **2010**, *119*, 202.
(9) Regnault, S.; Thiebaud, M.; Dumay, E.; Cheftel, J. C. *Int. Dairy J.* **2004**, *14*, 55.
(10) Gebhardt, R.; Doster, W.; Friedrich, J.; Kulozik, U. *Eur. Biophys. J.* **2006**, *35*, 503.
(11) Gebhardt, R.; Doster, W.; Kulozik, U. *Braz. J. Med. Biol. Res.* **2005**, *38*, 1209.
(12) Panick, G.; Vidugiris, G. J. A.; Malessa, R.; Rapp, G.; Winter, R.; Royer, C. A. *Biochemistry* **1999**, *38*, 4157.
(13) Daniel, I.; Oger, P.; Winter, R. *Chem. Soc. Rev.* **2006**, *35*, 858.
(14) Gebhardt, R.; Hanfland, M.; Mezouar, M.; Riekel, C. *Biomacromolecules* **2007**, *8*, 2092.
(15) Doster, W.; Gebhardt, R. *Chem. Phys.* **2003**, *292*, 383.
(16) Appavou, M. S.; Gibrat, G.; Bellissent-Funel, M. C. *Biochim. Biophys. Acta, Proteins Proteomics* **2006**, *1764*, 414.
(17) Calandrini, V.; Hamon, V.; Hinsen, K.; Calligari, P.; Bellissent-Funel, M. C.; Kneller, G. R. *Chem. Phys.* **2008**, *345*, 289.
(18) Bispo, J. A. C.; Santos, J. L. R.; Landini, G. F.; Goncalves, J. M.; Bonafe, C. F. S. *Biophys. Chem.* **2007**, *125*, 341.
(19) Santos, J. L. R.; Aparicio, R.; Joekes, I.; Silva, J. L.; Bispo, J. A. C.; Bonafe, C. F. S. *Biophys. Chem.* **2008**, *134*, 214.
(20) Schulte, A.; Buchter, S.; Galkin, O.; Williams, C. *J. Am. Chem. Soc.* **1995**, *117*, 10149.
(21) Gebhardt, R.; Vendrely, C.; Hanfland, M.; Riekel, C. *Macromolecules* **2008**, *41*, 9934.
(22) Herberhold, H.; Marchal, S.; Lange, R.; Scheyhing, C. H.; Vogel, R. F.; Winter, R. *J. Mol. Biol.* **2003**, *330*, 1153.
(23) Molina-Hoppner, A.; Doster, W.; Vogel, R. F.; Ganzle, M. G. *Appl. Environ. Microbiol.* **2004**, *70*, 2013.
(24) Dirix, C.; Duvetter, T.; Loey, A. V.; Hendrickx, M.; Heremans, K. *Biochem. J.* **2005**, *392*, 565.
(25) Smeller, L.; Meersman, F.; Heremans, K. *Eur. Biophys. J.* **2008**, *37*, 1127.
(26) Dzwolak, W.; Ravindra, R.; Lendermann, J.; Winter, R. *Biochemistry* **2003**, *42*, 11347.
(27) Doster, W.; Friedrich, F. *Protein Folding Handbook*; Wiley: New York, 2005.
(28) Tolkach, A.; Kulozik, U. *J. Food Eng.* **2005**, *67*, 13.
(29) Först, P.; Werner, F.; Delgado, A. *Rheol. Acta* **2000**, *39*, 566.
(30) Wong, P.; Moffat, D.; Baudais, F. *Appl. Spectrosc.* **1985**, *39*, 733.
(31) de Kruif, C. G. *J. Dairy Sci.* **1998**, *81*, 3019.
(32) Takeda, N.; Kato, M.; Taniguchi, Y. *Biochemistry* **1995**, *34*, 5980.
(33) Cheng, H.; Nikolic-Hughes, I.; Wang, J. H.; Deng, H.; O'Brien, P. J.; Wu, L.; Zhang, Z.-Y.; Herschlag, D.; Callender, R. *J. Am. Chem. Soc.* **2002**, *124*, 11295.
(34) Holt, C.; Davies, D. T.; Law, A. J. R. *J. Dairy Res.* **1986**, *53*, 557.
(35) O'Connell, J. E.; Grinberg, V. Y.; de Kruif, C. G. *J. Colloid Interface Sci.* **2003**, *258*, 33.
(36) Evans, D. F.; Wennerström, H. *The Colloidal Domain*; Wiley-VCH: New York, 1999.
(37) Lin, S. H. C.; Leong, S. L.; Dewan, R. K.; Bloomfield, V. A.; Morr, C. V. *Biochemistry* **1972**, *11*, 1818.
(38) Kulozik, U. *J. Membr. Sci.* **1998**, *145*, 91.
(39) Schmitz, K. S. *Dynamic Light Scattering by Macromolecules*; Academic Press: New York, **1990**; pp 20, 77.